Protonation states of intermediates in the reaction mechanism of [NiFe] hydrogenase studied by computational methods.

Dong, Geng; Ryde, Ulf

Published in:
Journal of Biological Inorganic Chemistry

DOI:
10.1007/s00775-016-1348-9

2016

Document Version:
Peer reviewed version (aka post-print)

Protonation states of intermediates in the reaction mechanism of [NiFe] hydrogenase studied by computational methods

Geng Dong, Ulf Ryde *

Department of Theoretical Chemistry, Lund University, Chemical Centre, P.O. Box 124, SE-221 00 Lund, Sweden

Correspondence to Ulf Ryde, E-mail: Ulf.Ryde@teokem.lu.se,
Tel: +46 – 46 2224502, Fax: +46 – 46 2228648

2015-10-01

Abstract

The [NiFe] hydrogenases catalyse the reversible conversion of H_2 to protons and electrons. The active site consists of a Fe ion with one carbon monoxide, two cyanide, and two cysteine (Cys) ligands. The latter two bridge to a Ni ion, which has two additional terminal Cys ligands. It has been suggested that one of the Cys residues is protonated during the reaction mechanism. We have used combined quantum mechanical and molecular mechanics (QM/MM) geometry optimisations, large QM calculations with 817 atoms, and QM/MM free energy simulations, using the TPSS and B3LYP methods with basis sets extrapolated to the quadruple zeta level to determine which of the four Cys residues is more favourable to protonate for four putative states in the reaction mechanism, Ni-SI_a, Ni-R, Ni-C, and Ni-L. The calculations show that for all states, the terminal Cys-546 residue is most easily protonated by 14–51 kJ/mol, owing to a more favourable hydrogen-bond pattern around this residue in the protein.

Keywords: [NiFe] hydrogenase, protonation, reaction mechanism, QM/MM, big-QM calculations, QM/MM free-energy perturbation, QTCP, density functional theory.

INTRODUCTION

Hydrogenases are enzymes that catalyse the reversible conversion of protons and electrons to H_2. The industrial process of H_2 generation requires high temperature [1], whereas the enzymes can catalyse this process at ambient temperature and pressure. During the latest decade, the hydrogenases have attracted much interest owing to their potential use in non-carbon based renewable energy production, employing H_2 both as an energy carrier and a transportable fuel [1-6].

Hydrogenases are found in several groups of bacteria, archaea, and a few eukaryotes [7]. There are three types of hydrogenases in nature, differing in the metal content of the active site, viz. [NiFe], [FeFe], and [Fe] hydrogenases. Numerous crystal structures of hydrogenases have been presented [8]. The binuclear active site of [NiFe] hydrogenases is shown in Figure 1. The iron ion is coordinated by one carbon monoxide and two cyanide molecules. In addition, two thiolates from Cys-84 and 549 (the residues are numbered according to the enzyme from *Desulfovibrio vulgaris* Miyazaki F [9]) bridge the two metals. The nickel ion has two additional cysteine ligands (Cys-81 and 546) that are terminally coordinated. The enzyme typically also contains three FeS clusters and an octahedral Mg^{2+} site.

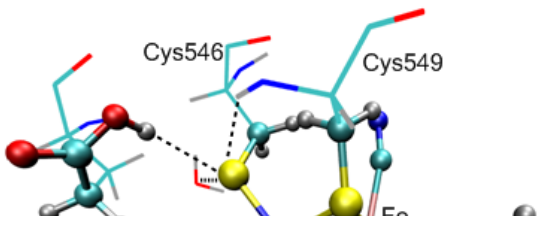

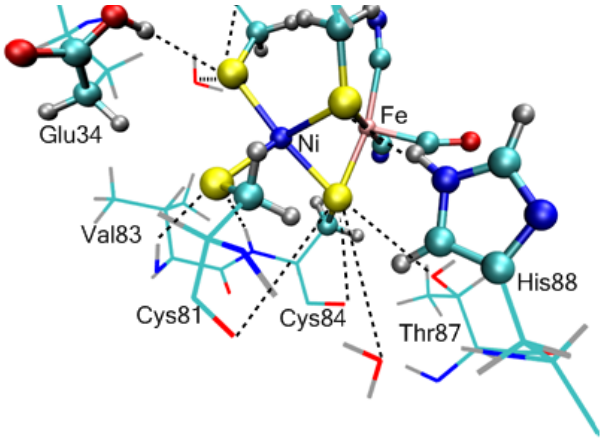

Figure 1. The active site of the [NiFe] hydrogenase. The atoms shown in the ball-and-stick mode were considered by QM methods in the QM/MM calculations.

The [NiFe] hydrogenases have been thoroughly studied by spectroscopic [7, 10, 11], electrochemical [12], biomimetic [13, 14], and computational methods [15-20]. These have identified a number of intermediates in the reaction and allowed for the suggestion of the putative reaction mechanism shown in Figure 2 [7]. The actual catalytic cycle involves only three states, starting with Ni-SI_a, in which the Ni ion is in the +II oxidation state, without any additional ligands (the Fe ions remains in the low-spin +II state throughout the reaction). This state binds H_2 and directly cleaves the H–H bond to give a bridging hydride ion and a protonated Cys residue in the fully reduced Ni-R state. In the next step, the active site is oxidised to Ni(III) and the proton on the Cys residue is transferred to solution, giving the Ni-C state. Finally, another electron is transferred away from active site, leading to a conversion of the bridging hydride ion to a proton that is also transferred to solution, probably via a Cys residue, returning the active site to the Ni-SI_a state. The Ni-C state is photolabile and can be converted to another state, Ni-L by exposure to visible light at cryogenic temperatures [21-25]. In this paramagnetic state, the bridging hydride ligand has been lost [7]. Recently, the Ni-L state was found also in the dark environment [26, 27], suggesting that this species may be a catalytic intermediate of the [NiFe] hydrogenases.

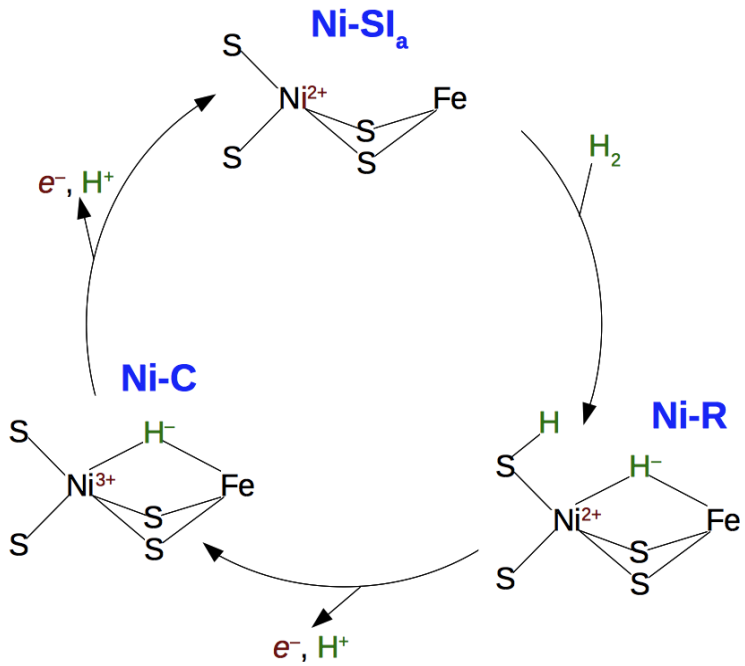

Figure 2. The consensus reaction mechanism of the [NiFe] hydrogenases, involving the Ni-SI_a, Ni-R, and Ni-C states [7].

Consequently, the reaction mechanism involves the protonation of some of the Cys ligands. Early QM-cluster studies suggested that the bridging Cys-549 is protonated [28]. However, more recent studies have typically assumed that the terminal Cys-546 is protonated, at least if His-88 (which forms a hydrogen bond to Cys-549) is positively charged [17, 29]. These two residues are also connected to the surface of the protein through proton-transfer pathways involving His-88 and His-484 in the former case and Glu-34 in the latter case [17, 30-33]. On the other hand, Neese and coworkers only considered protonation of the two terminal Cys ligands and found that a protonated

also connected to the surface of the protein through proton-transfer pathways involving His-88 and His-484 in the former case and Glu-34 in the latter case [17, 30-33]. On the other hand, Neese and coworkers only considered protonation of the two terminal Cys ligands and found that a protonated Cys-546 reproduced the experimental vibrational frequency shifts better for the Ni-R state, whereas both residues gave similar results for the Ni-SI_a state [19]. Very recently, they showed that both terminal protonations reproduced the nuclear resonance vibrational spectroscopy of the Ni-R state equally well [34]. Bruschi et al. also considered only protonation of the two terminal Cys residues and concluded that Cys-546 gives the more favourable energies, although no quantitative data were provided [20]. On the other hand, Hall and coworkers suggested that Cys-81 is protonated throughout the catalytic cycle, whereas Cys-546 is intermittently also protonated [35]. In particular, protonation of Cys-81 was found to be more favourable than protonation of Cys-546 for the Ni-SI state [36]. Amara et al. suggested that the terminal Cys-81 is protonated in the Ni-C state, whereas the other terminal Cys-546 is protonated in the Ni-R state [37], whereas Stein and Lubitz instead suggested a water molecule as the proton acceptor [38].

Ten years ago, we studied systematically which of the Cys residues is most likely to take up the proton [39]. We employed combined quantum-mechanical (QM) and molecular mechanics (MM) calculations (QM/MM), as well a joint QM/MM and crystallographic refinement, giving structures that are an optimum compromise between crystallography and QM and often allowing to deduce the protonation of metal ligands [40-42]. Unfortunately, it turned out that the available crystal structure were heavily affected by photo-reduction and contained a mixture of different oxidation states of the Ni ion, making it impossible to deduce which Cys ligand is protonated. Moreover, the protonation energies were extremely sensitive to details in the theoretical calculations (in particular the size of the QM system and the treatment of the surroundings), again making it hard to settle which of the Cys ligands is most easily protonated. Since then, we have in a series of publications examined the problem and suggested improved methods involving QM/MM free-energy perturbations and calculations with very large QM systems [43-51]. The time is now ripe to apply these methods to study the protonation state of [NiFe] hydrogenase in the various states during the reaction cycle.

Very recently, a new crystal structure of [NiFe] hydrogenase was published with a resolution of 0.89 Å [52]. At this very high resolution, hydrogen atoms start to be visible. The data were collected for an almost pure (96%) pure Ni-R state and the structure shows a bridging hydride ion and a protonated Cys-546 residue. This allows us to calibrate our methods – they should reproduce this protonation preference for the Ni-R state. However, our calculations allow us to study also the other states in the reaction mechanism, including some putative intermediate states between those shown in Figure 2. This would provide a more complete view of the protonation preferences of the [NiFe] hydrogenase active site.

METHODS

The protein

All calculations were based on the 1.4-Å crystal structure of [NiFe] hydrogenase from *Desulfovibrio vulgaris* Miyazaki F [9] (PDB code 1H2R; the study was started long before the recent atomic-resolution structure of the same enzyme was published [52]). There are two subunits in this enzyme, S and L, and both were included in the calculations. The SO and one of the CO Fe ligands were replaced by CN^- ions to give a functional active site with the normal Fe ligands, as in previous computational studies of this enzyme [18, 19].

The setup of the enzyme was the same as in our previous calculation [47]. The protonation states of all the residues were determined by using PROPKA [53], H++ [54], a study of the hydrogen-bond pattern around the His residues, the solvent accessibility, and the possible formation of ionic pairs. All Arg, Lys, Asp, and Glu residues were assumed to be charged, except Glu-S16, Glu-S75, and Glu-34 (an initial "S" refers to the small subunit, whereas residue numbers without this letter refer to the large subunit). Glu-34 forms a hydrogen bond to the terminal Ni ligand Cys-546 (3.3 Å; cf. Figure 1) and it has been modelled in the protonated form in most previous computational studies (when included), with the proton pointing towards Cys-546 [17, 39, 47-49]. However, Neese and coworkers put the proton on the other oxygen atom [18], giving a repulsive interaction between Glu-34 and Cys-546, whereas Bruschi et al. assumed that Glu-34 is deprotonated and therefore could accept a proton from Cys-546 [20]. Glu-S16 interacts with the other carboxylate atom of Glu-34 via Thr-S18 [47]. Glu-S75 forms a hydrogen bond to one of the sulfide ions of the proximal [4Fe–4S] cluster. Cysteine ligands coordinating to metals were deprotonated. Among the His residues, His-S247, and 552 were protonated on the ND1atom, His-S45, S188, 36 75, 88, 127, 130, 132, 195, 235, 338, 351, and 484 were assumed to be protonated on NE2 atom, whereas the others (all on the surface of the enzyme) were assumed to be doubly protonated. His-88 forms a hydrogen bond to the bridging Cys-549 ligand (Figure 1) and our

S45, S188, 36 75, 88, 127, 130, 132, 195, 235, 338, 351, and 484 were assumed to be protonated on NE2 atom, whereas the others (all on the surface of the enzyme) were assumed to be doubly protonated. His-88 forms a hydrogen bond to the bridging Cys-549 ligand (Figure 1) and our protonation is in accordance with a detailed comparison between experimental and computational spectroscopic properties [18], as well as the recent atomic-resolution crystal structure [52]. On the other hand, Siegbahn and coworkers sometimes modelled it as doubly protonated [17].

The protein was protonated and solvated with water molecules forming a sphere with a radius of 53 Å around the geometric centre using the leap module of the Amber software package (~57 000 atoms in total) [55]. The added protons and water molecules were optimised by a 120 ps simulated annealing calculation, followed by a minimisation, keeping the other atoms fixed at the crystal-structure positions.

QM calculations

All QM calculations were performed with the Turbomole 6.5 software [56]. We employed two density-functional theory (DFT) methods, TPSS [57] and B3LYP [58-60], and three different basis sets of increasing size, def2-SV(P) [61], def2-TZVP [62], and def2-QZVPD [62, 63]. The calculations were sped up by expanding the Coulomb interactions in an auxiliary basis set, the resolution-of-identity (RI) approximation [64, 65]. Most calculations used a QM system consisting of the Ni and Fe ions with all their first-sphere ligands (CO, two CN^-, and four Cys residues, modelled by CH_3S^-), as well as an acetic-acid model of Glu-34 and an imidazole model of His-88 (shown as the ball-and-stick model in Figure 1). The Fe ion was always in the low-spin Fe(II) state, whereas the oxidation state for the Ni ion varied, although it was always kept in the low-spin state [34, 51]. Unrestricted formalism was used for the open-shell systems. Entropic and thermal corrections to ΔG (at 298.15 K and 1 atm pressure) were calculated from harmonic frequencies of this QM system optimised in vacuum without any constraints.

QM/MM calculations

The QM/MM calculations were performed with the ComQum software [66, 67]. In this approach, the protein and solvent are split into three subsystems: System 1 (the QM system) was relaxed by QM methods. It contained the same atoms as the vacuum QM calculations. System 2 consisted of all residues or water molecules within 6 Å of any atom in system 1 and was relaxed by a full MM minimisation in each step of the QM/MM geometry optimisation in some of the calculations. Finally, system 3 contained the remaining part of the protein and the solvent. It was kept fixed at the original (crystallographic) coordinates.

In the QM calculation, system 1 was represented by a wavefunction, whereas all the other atoms were represented by an array of partial point charge, one for each atom, taken from MM libraries. Thereby, the polarisation of the QM system by the surroundings is included in a self-consistent manner (electrostatic embedding). When there is a bond between systems 1 and 2 (a junction), the hydrogen link-atom approach was employed: The QM system was capped with hydrogen atoms (hydrogen link atoms, HL), the positions of which are linearly related to the corresponding carbon atoms (carbon link atoms, CL) in the full system [66, 68]. All atoms were included in the point-charge model, except the CL atoms [46].

The total QM/MM energy in ComQum was calculated as [66, 67]

(1)

where is the QM energy of the QM system truncated by HL atoms and embedded in the set of point charges modelling systems 2 and 3 (but excluding the self-energy of the point charges). is the MM energy of the QM system, still truncated by HL atoms, but without any electrostatic interactions. Finally, is the classical energy of all atoms in the system with CL atoms and with the charges of the QM system set to zero (to avoid double counting of the electrostatic interactions). By this approach, which is similar to the one used in the ONIOM method [69], errors caused by the truncation of the QM system should cancel.

The geometry optimisations were continued until the energy change between two iterations was less than 2.6 J/mol (10^{-6} a.u.) and the maximum norm of the Cartesian gradients was below 10^{-3} a.u. The QM calculations were carried out using Turbomole 6.5 software [56]. Geometry optimisation were performed using the TPSS [57] functional in combination with def2-SV(P) [61]basis set, including empirical dispersion corrections with the DFT-D3 approach, as implemented in Turbomole [70]. The MM calculations were performed with the Amber software [55], using the Amber ff14SB force field [71].

Big-QM calculation

Previous studies of [NiFe] hydrogenase have shown that both QM-cluster and QM/MM energies strongly depend on the size of the studied QM system [45, 46]. To avoid this problem, we have

Big-QM calculation

Previous studies of [NiFe] hydrogenase have shown that both QM-cluster and QM/MM energies strongly depend on the size of the studied QM system [45, 46]. To avoid this problem, we have developed the big-QM approach to obtain converged results [47]: The minimal QM system, consisting of the two metal ions and their first-sphere ligands, was extended with all residues with at least one atom within 4.5 Å and junctions were moved at least two residues away. In addition, all charged groups buried inside the protein were included, but the three iron–sulfur clusters were omitted to avoid convergence problems, which according to our previous calculations can be done without compromising the energies [47, 48]. This gave a QM system of 817 atoms, shown in Figure 3. The big-QM calculations were performed on coordinates from the QM/MM calculations and with a point-charge model of the surroundings because this gave the fastest calculations in our previous tests [47]. They also employed the multipole-accelerated resolution-of-identity J approach (marij keyword).

To this big-QM energy, we added the DFT-D3 dispersion correction, calculated for the same big QM system with Becke–Johnson damping [72], third-order terms, and default parameters for the TPSS functional using dftd3 program [70]. We also included a standard QM/MM MM correction for this large QM system:

(2)

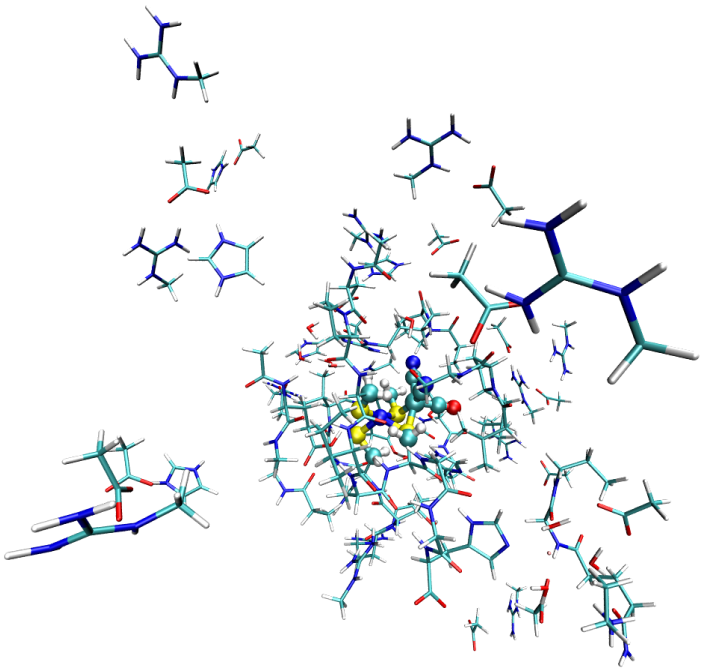

Figure 3. Atoms included in the big-QM calculations.

QTCP calculations

The QTCP approach (QM/MM thermodynamic cycle perturbation) is a method to calculate free energies between the two states A and B with a high-level QM/MM method, using sampling at only the MM level [43, 44, 73]. It employs the thermodynamic cycle shown in Figure 4. In this approach, free-energy difference between A and B is described by three terms:

(3)

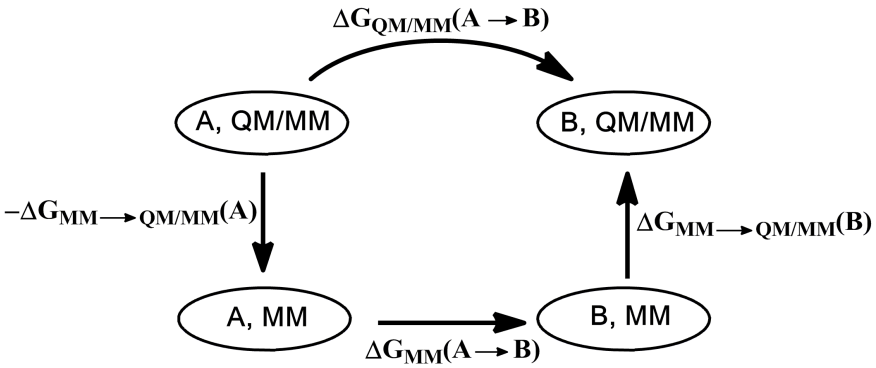

Figure 4. The thermodynamic cycle employed in the QTCP calculations.

The QTCP calculations were performed as has been described before [43, 44, 74]: First, each state of interest was optimised by QM/MM, keeping system 2 fixed at the crystal structure. Then, the protein was further solvated in an octahedral box of TIP3P water molecules [75], extending at least 9 Å from the QM/MM system. For the A state, the system was first subjected to a 1000-step

The QTCP calculations were performed as has been described before [42, 43, 44]. First, each state of interest was optimised by QM/MM, keeping system 2 fixed at the crystal structure. Then, the protein was further solvated in an octahedral box of TIP3P water molecules [75], extending at least 9 Å from the QM/MM system. For the A state, the system was first subjected to a 1000-step minimisation, keeping the atoms in the QM part fixed and restraining all heavy atoms from the crystal structure with a force constant of 418 kJ/mol/Å^2. Then, two 20 ps MD simulations were run with the heavy atoms still restrained. The first was run with a constant volume, the second with a constant pressure. Next, the size of the periodic box was equilibrated by a 100-ps MD simulation with a constant pressure and only the heavy atoms in QM system restrained to the QM/MM structure. The final structure of this simulation was used as the starting structure also for the other state. Finally, an equilibration of 200 ps and a production of 400 ps were run with a constant volume for each state. During the production run, 200 snapshots were collected every 2 ps.

Based on these snapshots, three sets of free-energy perturbations (FEPs) were performed as is shown in Figure 4. First, FEPs were performed at the MM level in the forward and reverse direction along the reaction coordinate by changing the charges and coordinates of the QM system to those of the QM/MM calculations [74]. Charges were first modified in nine steps, keeping the coordinates at those of the A state. Then, the coordinates were modified in five steps to those of the B state (with all charges in the B state). Second, MM®QM/MM FEPs were performed for both the A and B states, keeping the QM systems fixed, as has been described before [43, 44]. All FEP calculations were performed with the local software calcqtcp. Further details of the QTCP calculations can be found in http://www.teokem.lu.se/~ulf/Methods/qtcp.html.

Reported energies are the big-QM energies obtained with TPSS/def2-TZVP on the QM/MM structures obtained with system 2 relaxed, including dispersion and MM corrections (). This energy was extrapolated to the B3LYP/def2-QZVPD level of theory using QM calculations of the normal QM system and a point-charge model (). To this, the QTCP energy correction (i.e. the difference between the QTCP and QM/MM energies,) was added, as well as the thermal and entropic corrections to ΔG of the normal QM system, obtained from the frequency calculation at the TPSS/def2-SV(P) level in vacuum, without any constraints ():

(4)

The various energy components, obtained with or without system 2 relaxed are collected in Tables S1–S4 in the supplementary material.

RESULTS AND DISCUSSION

In this paper, we focus on four states of [NiFe] hydrogenase, viz. the Ni-SI$_a$, Ni-R, Ni-C, and Ni-L states. For these states, we will discuss which of the active-site Cys residues is most likely to be protonated by estimating the relative energies of the various protonation states. Thus, we have for each state studied both the state with all four Cys residues deprotonated and the four states with one of the Cys ligands protonated.

We started with an analysis of the starting crystal structure [9] to deduce possible positions of protonation for the various Cys residues. From Figure 1, it can be seen that Cys-81 binds to the Ni ion and receives two hydrogen bonds from the backbone N groups of Val-83 and Cys-84 (S–N distances of 3.3–3.4 Å). If this Cys is protonated, the proton must be directed away from these three groups, but the closest hydrogen-bond acceptor in that direction is the carboxylate group of Glu-34, at a S–O distance of 4.6 Å. Cys-546 coordinates to Ni and forms a favourable hydrogen bond to the protonated carboxylate group of Glu-34 (S–O distance of 3.3 Å; cf. Figure 1). It also forms a weaker interaction with the backbone N group of Cys-549 (S–N distance 4.2 Å), again giving only a single site for a possible protonation. In that direction, there is a crystal water molecule at a S–O distance of 3.7 Å, providing a possible hydrogen-bond acceptor. Cys-549 bridges between the Ni and Fe ions and forms a strong hydrogen bond to the side chain of His-88 (S–N distance 3.3 Å; Figure 1), giving also a single possible site for protonation. However, this direction is quite crowded with no natural hydrogen-bond acceptors. Finally, Cys-84 is also bridging the two metal ions, but it does not form any clear hydrogen bonds to the surrounding protein. The side-chain OG1 atom of Thr-87 is at an S–O distance of 3.6 Å, but the proton points in another direction in our starting structure (cf. Figure 1). This would give two possible sites of protonation of Cys-84, but one of these would bring the proton quite close to the already protonated NE2 of His-88 (S–N distance of 4.0 Å). In the other direction, there are the backbone O atom of Cys-84 and OG1 atom of Thr-87, which both could act as hydrogen-bond acceptors at S–O distances of 3.0 and 3.6 Å, respectively. In this neighbourhood, there are also the backbone O atom of Cys-81 and a crystal water molecule at S–O distances of 5.0 and 4.8 Å, respectively. Based on these considerations, we tested one protonation site for each of the four Cys residues to see which gives lowest energy. We first discuss the obtained structures and then compare the energies of the various protonation states.

Structures

four Cys residues to see which gives lowest energy. We first discuss the obtained structures and then compare the energies of the various protonation states.

Structures

In the Ni-SI$_a$ state, the two active-site ions are in the Ni(II) and Fe(II) oxidation states and we have assumed that both are in the closed-shell low-spin state [34, 51]. The structures of this species in the various protonation states (deprotonated or protonated on each of the four Cys residues) are shown in Figure 5, with the Ni–Fe and the various metal–ligand distances indicated.

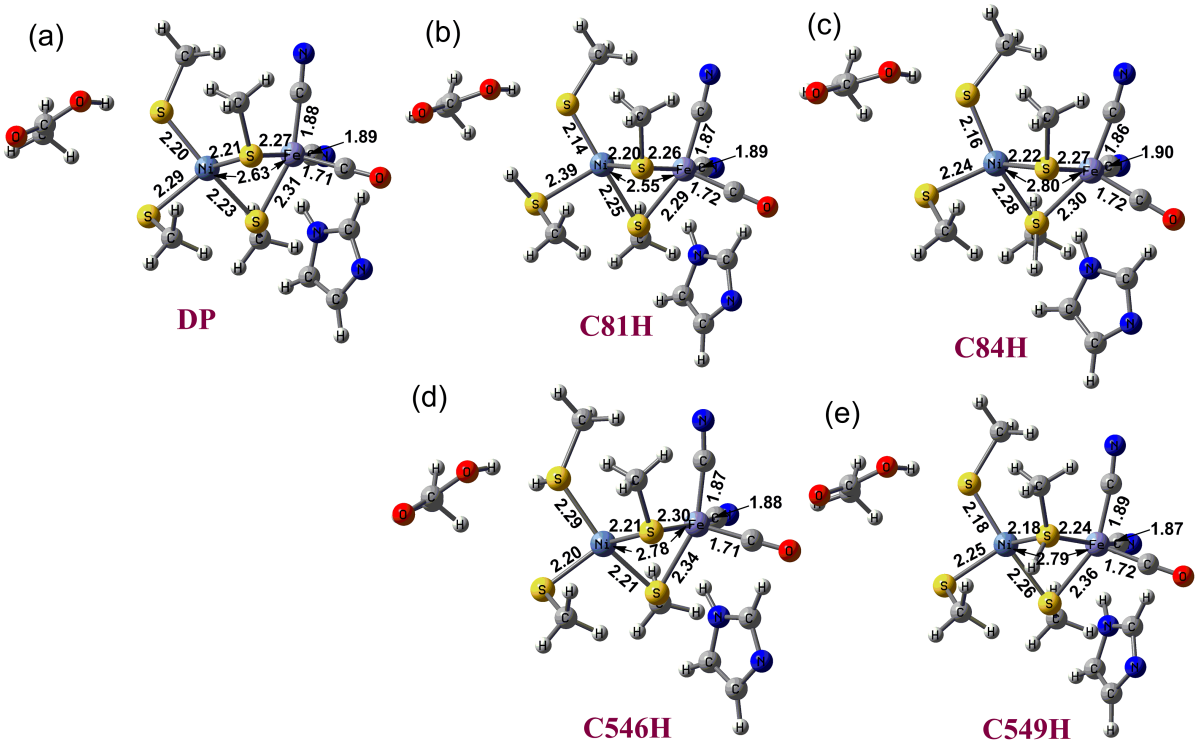

Figure 5. Structures and bond lengths in the various protonation states of Ni-SI$_a$ state.

The structures change somewhat when the various Cys groups are protonated. If a terminal Cys residue is protonated, the corresponding Ni–S distance increases by ~0.1 Å, whereas the other terminal Ni–S distance decreases by 0.06–0.09 Å. The Ni–S and Fe–S distances of the bridging Cys residues decrease only slightly (by up to 0.02 Å) and sometimes even increase (by up to 0.03 Å). Likewise, if one of the bridging Cys residues is protonated, the Ni–S and Fe–S distances of the bridging Cys residues can both increase or decrease (by up to 0.05 Å), but the Ni–S distances to the terminal Cys always decrease by 0.02–0.05 Å. The Ni–Fe distance increases to ~2.79 Å in all states except when Cys-81 is protonated, in which case it decreases to 2.55 Å. The Fe–C bond lengths change by less than 0.02 Å.

According to the consensus mechanism of [NiFe] hydrogenase, H_2 binds to the Ni-SI$_a$ state and is rapidly cleaved to a proton and a hydride ion (cf. Figure 2) [7]. The former is bound to one of the four Cys ligands, whereas the latter bridges the two metal ions. This is the Ni-R state, which still contains a low-spin Ni(II) ion (the Fe ion was always modelled in the low-spin Fe(II) state). The structures of the various protonation states of Ni-R are presented in Figure 6. The presence of a bridging hydride ion leads to a shortening of the Ni–Fe bond to 2.53–2.59 Å in all states. Moreover, the Ni–S bond length to the bridging Cys-549 is elongated to 2.55–2.86 Å, making it distinctly longer than for the other Cys residues (2.16–2.28 Å), reflecting that it has become an axial ligand in a distorted square-pyramidal geometry. The Fe–S distance to Cys-549 (2.38–2.41 Å) is also longer than that to Cys-84 (2.23–2.29 Å), but the difference is smaller when Cys-549 is protonated (2.34 and 2.31 Å). The Fe–C distances typically increase by 0.01 Å compared to the Ni-SI$_a$ state. The Ni–H bond is appreciably shorter than the Fe–H bond, 1.56–1.61 Å, compared to 1.69–1.76 Å. In variance to the Ni-SI$_a$ state, protonation of the terminal Cys residues leads to a shortening of the corresponding Ni–S distance, whereas protonation of the bridging Cys-549 leads to a 0.13 Å elongation of that Ni–S bond and a 0.07 Å shortening of the Fe–S bond.

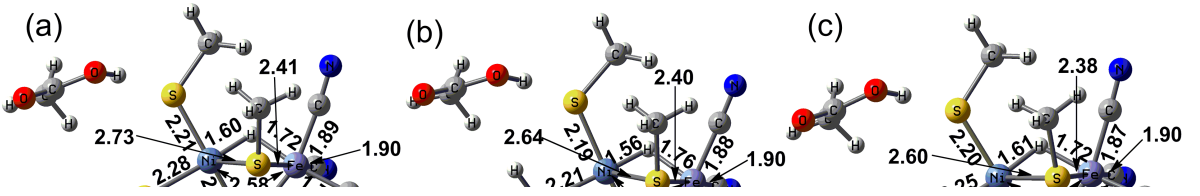

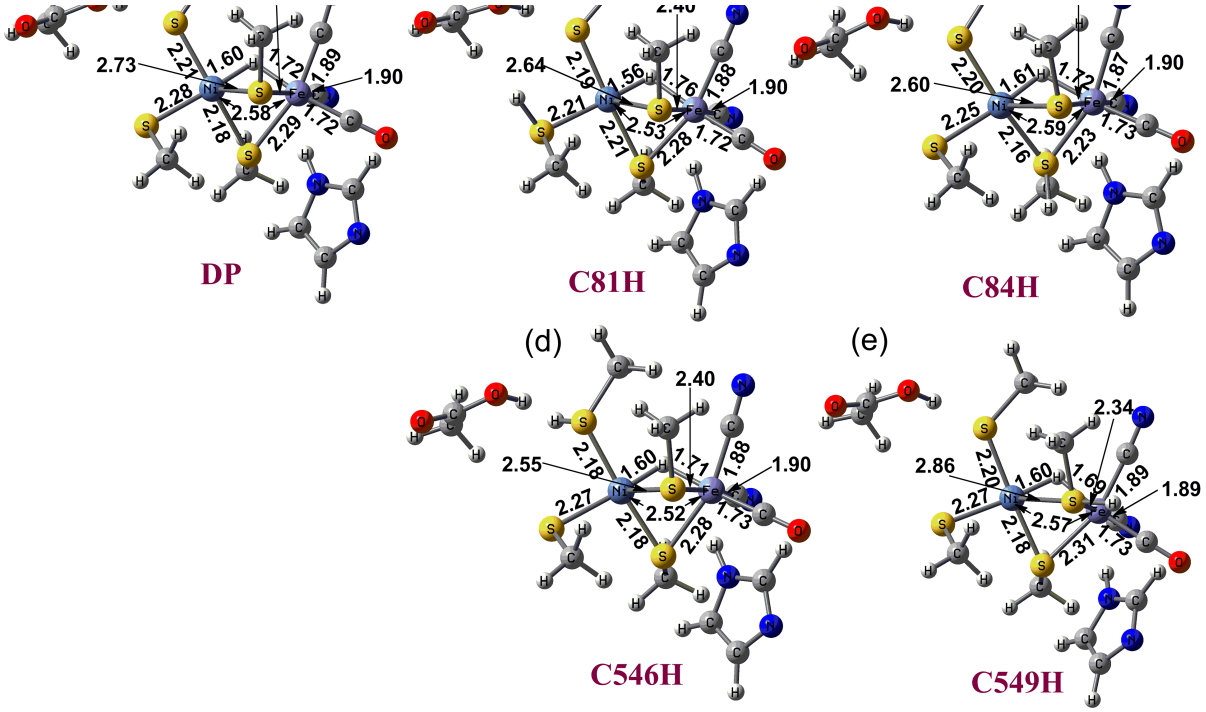

Figure 6. Structures and bond lengths in the various protonation states of Ni-R state.

In the Ni-C state, one electron has been removed from the Ni-R state, giving a Ni(III) ion, but the bridging hydride ion is still there. The structures of the various protonated states are shown in Figure 7. The Ni–Fe distance is typically slightly shorter than in the Ni-R state, 2.48–2.57 Å. The Ni–S distance is still longer for Cys-549 than for the other Cys residues, but the difference is much smaller than for the Ni-R state, 2.34–2.39 Å vs. 2.17–2.29 Å. In fact, the distance to Cys-546 is somewhat shorter than the other two distances, except when it is protonated (2.17–2.21 Å vs. 2.24–2.29 Å). The Ni–H bond is 0.01–0.05 Å longer than in the Ni-R state, whereas the Fe–H bond is typically somewhat shorter, making the two bond lengths more similar. Protonation of a Cys residue makes the corresponding Ni–S bond longer for all residues except Cys-549, whereas the corresponding Fe–S bonds always become shorter.

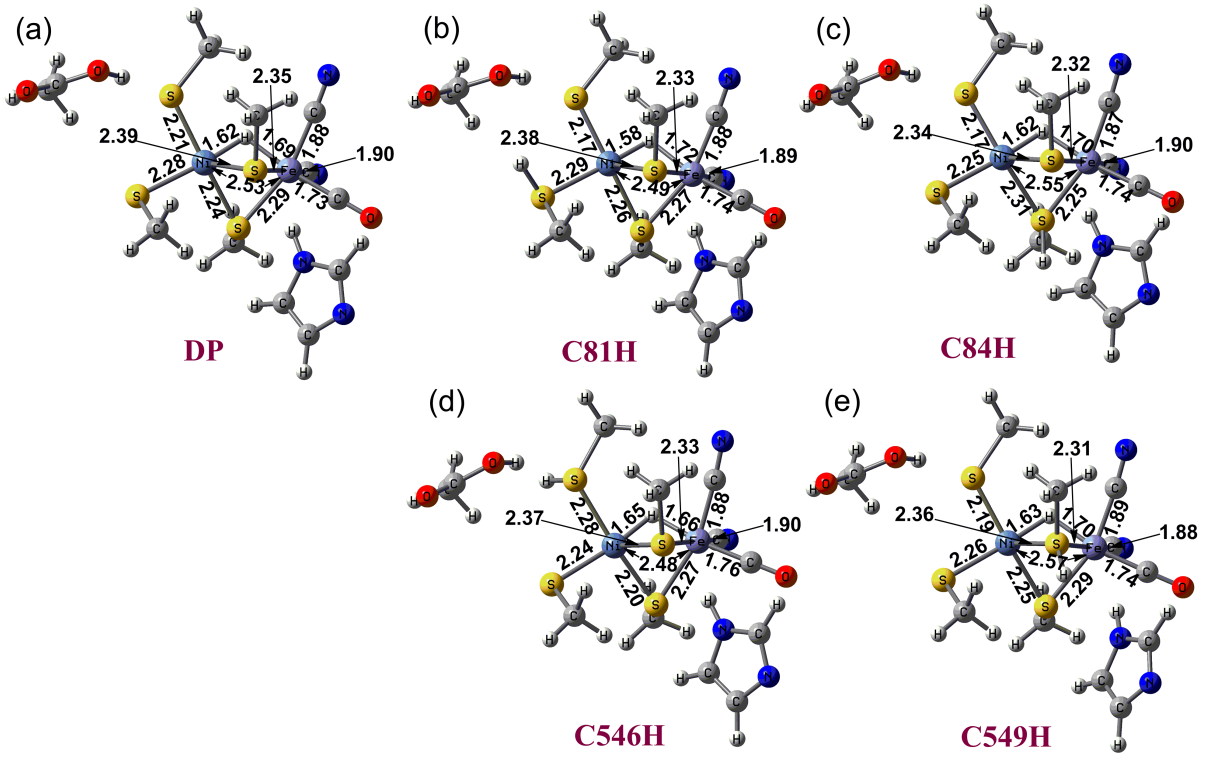

Figure 7. Structures and bond lengths in the various protonation states of Ni-C state.

Ni-L state is generated from Ni-C state by converting the bridging hydride to a proton. The two electrons on the hydride ion then reduces the Ni ion to the +I oxidation state [76]. The considered protonation states of Ni-L are shown in Figure 8. It can be seen that the Ni–Fe distance is slightly shorter than in the Ni–SI_a state, but longer than in the other two states. The Ni–S distances are rather similar, although there is a tendency that the distances of Cys-81 and 549 are somewhat longer than those of the other two Cys residues, except when Cys-549 is protonated (2.29–2.39 Å vs. 2.19–2.25

shorter than in the Ni–SI$_a$ state, but longer than in the other two states. The Ni–S distances are rather similar, although there is a tendency that the distances of Cys-81 and 549 are somewhat longer than those of the other two Cys residues, except when Cys-549 is protonated (2.29–2.39 Å vs. 2.19–2.25 Å). The same trend applies also to the Fe–S distances.

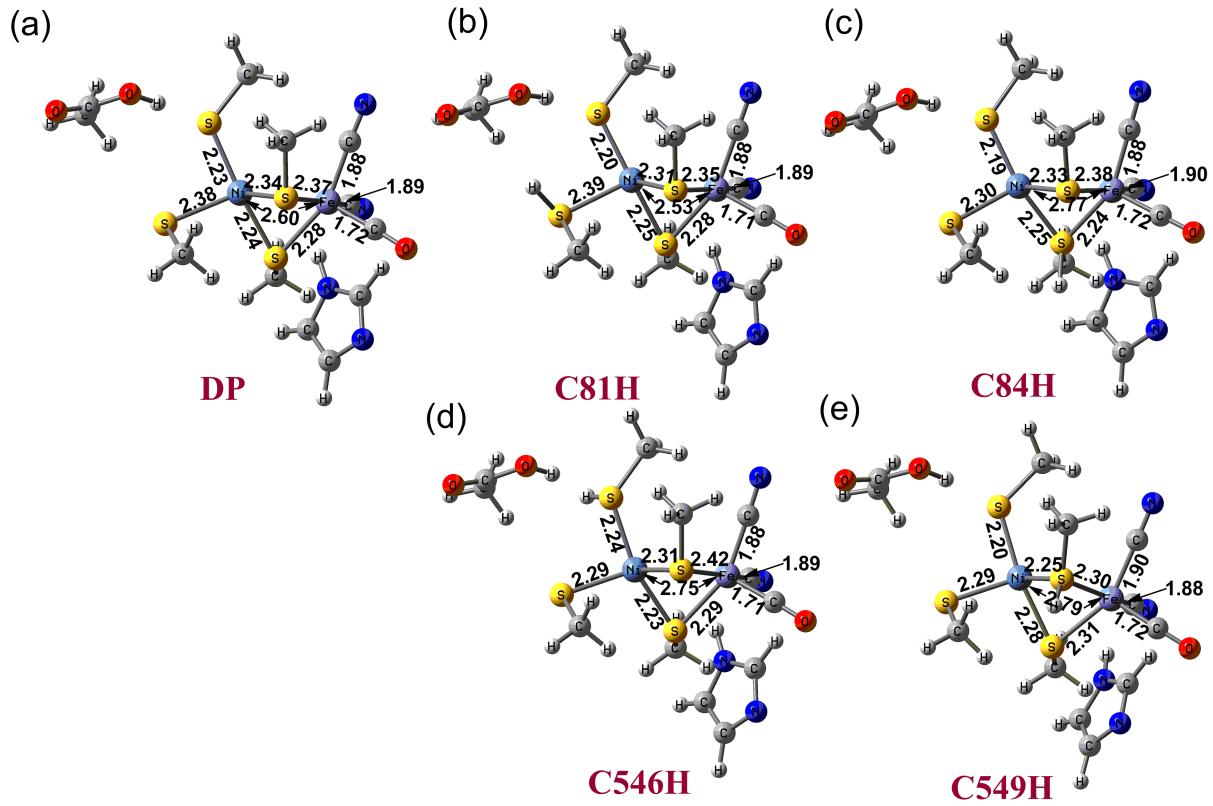

Figure 8. Structures and bond lengths in the various protonation states of Ni-L state.

Energies

Next, we focus on the energies: The energies of the four states with the various Cys residues protonated are directly comparable and can therefore be used to decide which is the most stable protonation state. Our final energies (calculated as is shown in Eqn. 4) for the protonated variants of the Ni-SI$_a$, Ni-R, Ni-C, and Ni-L states are collected in Table 1.

Table 1. The relative energies (kJ/mol) of the various protonated states for the four studied states of [NiFe] hydrogenase, obtained according to Eqn. 4.

Protonated	Ni-SI$_a$	Ni-R	Ni-C	Ni-L
Cys-81	0.0	0.0	0.0	0.0
Cys-84	77.9	47.2	46.4	38.5
Cys-546	-22.8	-13.8	-50.6	-32.5
Cys-549	105.3	17.3	33.0	61.6

For the Ni-R state, our results show that protonation of Cys-546 is most favourable, giving a state that is 14 kJ/mol more stable than protonation of Cys-81. Protonation on the bridging Cys-549 and 84 are disfavoured by 31 and 61 kJ/mol, respectively, confirming the intuitive expectation that it is easier to protonate a terminal Cys ligand than a bridging one (the bridging ligands coordinate to two positively charged metal ions, which are expected to stabilise the deprotonated ligand). The preferred protonation of Cys-546 is supported by the recent crystal structure of this state [52], increasing the credibility of the current results. Interpretation of the vibrational frequency shifts has also supported the protonation of Cys-546 in this state [19], and computational studies have favoured the same state if His-88 is positively charged [17, 29] or when Glu-34 is deprotonated [20]. The present calculations show that protonation of Cys-546 is most stable also with a neutral His-88 and a protonated Glu-34. Consequently, we can be quite confident that the present approach works and gives accurate estimates of the relative stability of the various protonated Cys residues also for the other states.

There are some subtle differences between the positions of the proton on Cys-546 in our QM/MM structure and in the recent crystal structure of this state [52]: The H^{γ}–S^{γ}–C^{β}–C^{α} torsion angle is somewhat smaller in the optimised structure, 82° compared to 118° in the crystal structure

the other states.

There are some subtle differences between the positions of the proton on Cys-546 in our QM/MM structure and in the recent crystal structure of this state [52]: The H^{γ}–S^{γ}–C^{β}–C^{α} torsion angle is somewhat smaller in the optimised structure, 82° compared to 118° in the crystal structure. The H^{γ}–hydride distance is also somewhat longer, 3.2 Å compared to 2.5 Å, but this is partly an effect of a dubious H^{γ}–S^{γ}–C^{β} angle of only 72° in the crystal structure (95° in the optimised structure). The S^{γ}–hydride distances are identical, 2.6 Å. We have reoptimised the QM/MM structure of the protonated R state, starting from the conformation in the 4U9H crystal structure, but it returns to the original QM/MM structure. The very low crystallographic B factor of the Cys-546 H^{γ} proton (1.6 compared to 7.0 for the S atom and 4.3–7.1 for the other H atoms in that residue) may indicate that it actually is a heavier atom, e.g. representing a partial oxidation of this residue.

The results in Table 1 show that also for the Ni-SI_a, Ni-C, and Ni-L states, protonation of Cys-546 is more favourable than protonation of the other three Cys residue, by 23–51 kJ/mol. In all cases, protonation of Cys-81 is also the second most stable state. However, the relative stability of protonation of the two bridging Cys residues varies with the states: For Ni-SI_a and Ni-L, Cys-84 is easier to protonate than Cys-549, but the opposite is true for Ni-C.

The results in Table 1 can be understood in terms of hydrogen bond around the Cys residues. The added proton on Cys-546 always form a strong hydrogen bond to a water molecule with a H–O distance of 2.0 Å in all four states (cf. Table S5). This also explains why protonation on Cys-546 is sensitive to the relaxation of the MM system (Tables S1–S4), because this water molecule has to change its hydrogen-bond network to ideally interact with the added proton. The added proton on Cys-84 forms a quite strong hydrogen bond to the backbone O of Cys-84 (2.1–2.3 Å) and a weaker hydrogen bond to the sidechain O atom of Thr-87 (2.8–3.0 Å), although the angles are far from ideal (S–H···O angles of ~120º and ~100º). However, protonation of this residue is intrinsically less favourable, because it bridges the two metal ions (e.g. by 84 kJ/mol for an isolated first-sphere Ni-SI_a model at the TPSS-D3/def2-QZVP level). The added proton on Cys-81 forms a rather week hydrogen bond to the protonated carboxylic acid O atom of Glu-34 (2.2–2.5 Å). Finally, the added proton on Cys-549 does not form any hydrogen bonds, but it is rather close to the $N^{\varepsilon 2}$ atom of His-88 (2.5–3.1 Å), which interferes with the hydrogen bond between the corresponding $H^{\varepsilon 2}$ atom and the S atom on Cys-546, making it 0.2–0.4 Å longer than in the deprotonated state. A similar elongation is also found for the hydrogen bond between the backbone H atom of Cys-84 and S of Cys-81 when both Cys-81 (0.2–0.3 Å elongation) and Cys-84 (0.3–0.5 Å elongation) are protonated. Likewise, the hydrogen bond between S in Cys-81 and the backbone H of Val-83 is elongated by 0.2–0.3 Å when Cys-81 is protonated, whereas the hydrogen bond between S in Cys-546 and the protonated carboxylate of Glu-34 is elongated only by 0.1–0.2 Å when Cys-546 is protonated. All together these variations in the hydrogen-bond patters selectively stabilise protonation of Cys-546.

The final energy estimates in Table 1 are composed of several energy contributions as is shown in Eqn. 4. These energy components are listed in Tables S1–S4 in the supplementary material. The final energies are based on the big-QM calculations with the 817-atom QM system in Figure 3 at the TPSS/def2-TZVP level. To this QM energy, a standard MM correction is added (to give a QM/MM energy), as well as DFT-D3 energy corrections, including third-order terms and Becke–Johnson damping. The dispersion correction to the relative energies is quite small, up to 13 kJ/mol. It is smaller for the Ni-R and Ni-C states than for the other two stated, especially when the MM system is fixed. In the latter case, the MM correction is also very small (1–3 kJ/mol), because only the normal QM system changes its coordinates, deep inside the big-QM system. However, when system 2 is relaxed, a much larger variation is seen (up to 46 kJ/mol), reflecting that many more atoms are moving.

The big-QM energies are then corrected for a larger basis set (def2-QZVPD) and a more accurate DFT method (B3LYP). The first correction is minimal (0–3 kJ/mol), because the def2-TZVP basis set is already almost converged. However, the second correction is larger, up to 16 kJ/mol. It is larger for the Ni-SI_a state than for the other states. The basis-set correction always disfavours protonation of Cys-81, but the sign of the method correction varies with the studied state.

We also added a QTCP correction (difference between the QTCP and QM/MM results, obtained at the TPSS/def2-SV(P) level. It amounts to –10 to 21 kJ/mol, always disfavouring protonation of the bridging Cys-84 and 549 residues. The QTCP energy contains free-energy corrections for the MM system, but not for the QM system (which was kept fixed in those calculations). Therefore, we finally added an entropic and thermal correction to ΔG of the QM system, amounting to –2 to 17 kJ/mol, always disfavouring protonation of Cys-549.

The relative big-QM energies change significantly when the MM system 2 is relaxed, but less for Ni-R (up to 19 kJ/mol) than for the other states (up to 34, 40, and 51 kJ/mol for Ni-SI_a, Ni-C, and Ni-L, respectively). Protonation of Cys-84 and 546 is always favoured. However, this change is to a large extent compensated by the MM energy, so that the QM/MM (–10 to 5 kJ/mol) and the MM+dispersion-corrected big-QM energies typically change appreciably less when the MM system

Ni-L, respectively). Protonation of Cys-84 and 546 is always favoured. However, this change is to a large extent compensated by the MM energy, so that the QM/MM (–10 to 5 kJ/mol) and the MM+dispersion-corrected big-QM energies typically change appreciably less when the MM system is relaxed, e.g. by up to 10 and 17 kJ/mol, respectively for the Ni-SI_a state.

Our results agree with the recent atomic-resolution crystal structure of the Ni-R state that the Cys-546 residue should be protonated [52]. However, in that structure, no proton is seen on Glu-34, although the O–S distance is only 3.4 Å. In our calculations, Glu-34 is protonated and forms a hydrogen bond to Cys-546. Therefore, we also performed some calculations in which Glu-34 was deprotonated and Cys-546 was protonated. However, in all such calculations, the proton was transferred from Cys-546 to Glu-34 during the optimisation, giving a structure identical to the state with all Cys residues deprotonated, indicating that a state with a deprotonated Glu-34 is unfavourable.

Likewise, we also performed some calculations with His-88 protonated on the $N^{\delta 1}$ atom (instead of the $N^{\varepsilon 2}$ atom as in all the other calculations). However, if Cys-549 was protonated, this proton was invariably transferred to His-88. Moreover, the used protonation state of His-88 is supported by the atomic-resolution crystal structure [52].

CONCLUDING REMARKS

In this paper, we have studied protonation of the four Cys ligands in the active site of [NiFe] hydrogenase with computational methods. Several earlier studies have shown that it is demanding to calculate accurate and reproducible energies for reactions in this enzyme [17, 18, 39, 45-48]. Therefore, we have used a set of advanced methods, partly developed with this enzyme as a test case: Geometries were optimised with a standard QM/MM method and a rather small active-site model (Figure 1). Then, accurate energies were calculated using the big-QM approach [47], including all chemical groups within 4.5 Å of the minimal active site, all buried charges, and moving junctions at least two residues away from the active site, in total 817 atoms (Figure 3). These calculations were performed at the TPSS/def2-TZVP level, but the energies were extrapolated to the B3LYP/def2-QZVPD level. Finally, we employed QM/MM free-energy simulations with the QTCP approach to avoid the local-minima problem for the QM/MM calculations and to obtain free energies. Calibration calculations have shown that by such an approach, energies with an accuracy of ~20 kJ/mol should be obtained [45-48].

With these methods we have compared the energies of protonation of each of the four Cys ligands for four states in the putative reaction mechanism of [NiFe] hydrogenase, Ni-SI_a, Ni-R, Ni-C, and Ni-L. The results show for all four states, protonation of the terminal Cys-546 is most favourable, by 14–51 kJ/mol. For the Ni-R state, this is in accordance with the recent atomic-resolution crystal structure of the enzyme [52], a computational interpretation of the vibrational spectra [19], and a DFT study of the H_2 binding and reaction mechanism [20]. However, for the other states, no consensus for the protonation has been reached and several conflicting assignments have been made [19, 28, 37].

The present results allow us to set up a detailed reaction mechanism, shown in Figure 9. The reaction starts with the deprotonated Ni-SI_a state with Ni in the +II oxidation state, which binds H_2. This H_2 adduct has not been observed; instead H_2 is heterolytically cleaved to a bridging hydride ion and a proton, which binds to Cys-546, the (protonated) Ni-R state. From this state, a proton and electron should be removed. If the proton is removed first, the deprotonated Ni-R state is obtained, shown in Figure 6. If instead, the electron is removed first, the protonated Ni-C state is obtained, which still is protonated on Cys-546, as is shown in Figure 7. However, in both cases, the end product is the (deprotonated) Ni-C state, with Ni in the +III oxidation state. Next, the hydride is converted to a proton, concomitant with the reduction of Ni to the +I state, giving the (protonated) Ni-L state. According to our calculations, this state should also be protonated on Cys-546. Finally, another electron and proton should be removed from this state. If the proton dissociates first, the deprotonated Ni-L state in Figure 8 is obtained. If instead the electron is removed first, the protonated Ni-SI_a state is obtained, still with Cys-546 is obtained. However, the final state is the (deprotonated) Ni-SI_a state, which is ready to start a new reaction cycle.

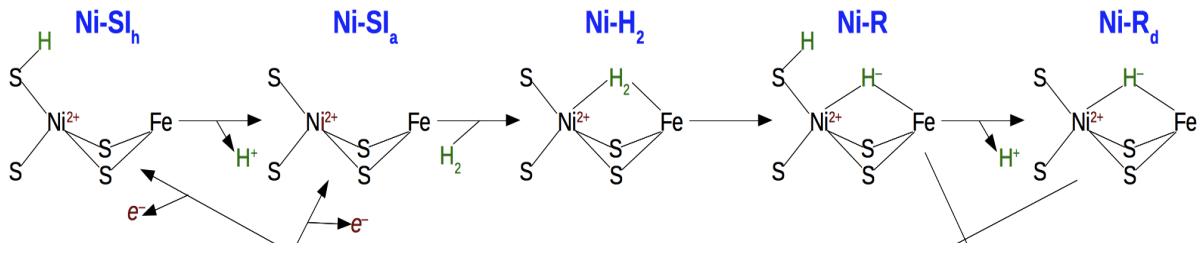

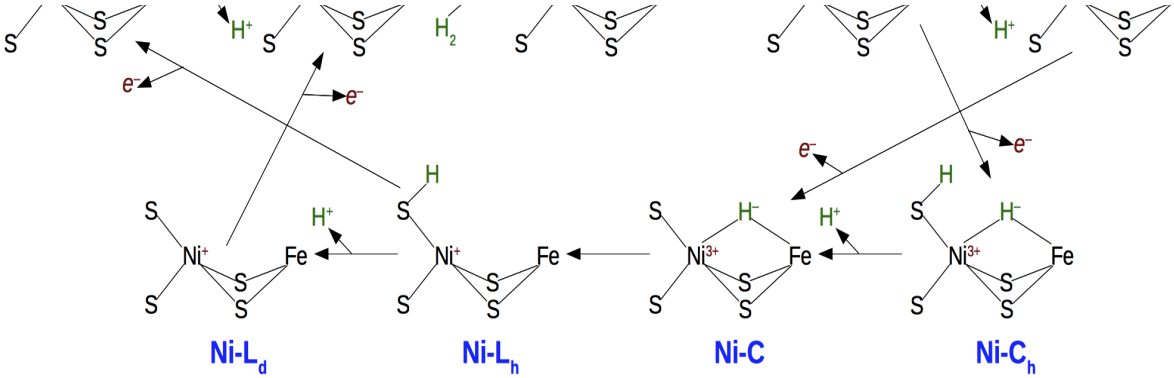

Figure 9. A putative reaction mechanism of [NiFe] hydrogenases involving all studied protonation states.

In this article, we have studied the protonated and deprotonated states in this putative mechanism. What remains is to study the H_2 binding, which complicated by the fact that different DFT methods give qualitatively different structures for the adduct (H_2 bridging the two metal ions, or coordinating to Fe or Ni) [17, 77]. Therefore, more advanced QM are needed [51]. Such studies are currently performed in our laboratory.

ACKNOWLEDGEMENTS

This investigation has been supported by grants from the Swedish research council (project 2014-5540), the China Scholarship Council, and COST through Action CM1305 (ECOSTBio). The computations were performed on computer resources provided by the Swedish National Infrastructure for Computing (SNIC) at Lunarc at Lund University.

1. Turner JA (1999) Science 285:687-689
2. Bockris JOM (2013) Int J Hydrogen Energy 38:2579-2588
3. Matsumoto T, Kim K, Nakai H, Hibino T, Ogo S (2013) Chemcatchem 5:1368-1373
4. Yang JY, Bullock M, DuBois MR, DuBois DL (2011) MRS Bull 36:39-47
5. Penner SS (2006) Energy 31:33-43
6. Cammack R, Frey M, Robson R (Eds) Hydrogen as a Fuel: Learning from Nature (Taylor & Francis, 2001),
7. Lubitz W, Ogata H, Ruediger O, Reijerse E (2014) Chem Rev 114:4081-4148
8. Fontecilla-Camps JC, Volbeda A, Cavazza C, Nicolet Y (2007) Chem Rev 107:4273-4303
9. Higuchi Y, Ogata H, Miki K, Yasuoka N, Yagi T (1999) Structure 7:549-556
10. De lacey AL, Fernandez VM, Rousset M, Cammack R (2007) Chem Rev 107:4304-4330
11. Lubitz W, Reijerse E, van Gastel M (2007) Chem Rev 107:4331-4365
12. Vincent KA, Parkin A, Armstrong FA (2007) Chem Rev 107:4366-4413
13. Tard C, Pickett CJ (2009) Chem Rev 109:2245-2274
14. Bakhmutov VI (2005) Eur J Inorg Chem, doi 10.1002/ejic.200400697:245-255
15. Fan H-J, Hall MB (2001) J Biol Inorg Chem 6:467-473
16. Bruschi M, Zampella G, Fantucci P, De Gioia L (2005) Coord Chem Rev 249:1620-1640
17. Siegbahn PEM, Tye JW, Hall MB (2007) Chem Rev 107:4414-4435
18. Kampa M, Lubitz W, van Gastel M, Neese F (2012) J Biol Inorg Chem 17:1269-1281
19. Kraemer T, Kamp M, Lubitz W, van Gastel M, Neese F (2013) Chembiochem 14:1898-1905
20. Bruschi M, Tiberti M, Guerra A, De Gioia L (2014) J Am Chem Soc 136:1803-1814
21. Pandelia M-E, Ogata H, Lubitz W (2010) Chemphyschem 11:1127-1140
22. Fichtner C, van Gastel M, Lubitz W (2003) Phys Chem Chem Phys 5:5507-5513
23. Medina M, Hatchikian EC, Cammack R (1996) Biochim Biophys Acta-Bioenerg 1275:227-236
24. Whitehead JP, Gurbiel RJ, Bagyinka C, Hoffman BM, Maroney MJ (1993) J Am Chem Soc 115:5629-5635
25. van der Zwaan JW, Albracht SPJ, Fontijn RD, Slater EC (1985) FEBS Lett 179:271-277
26. Hidalgo R, Ash PA, Healy AJ, Vincent KA (2015) Angewandte Chemie (International ed in English) 54:7110-7113
27. Murphy BJ, Hidalgo R, Roessler MM, Evans RM, Ash PA, Myers WK, Vincent KA, Armstrong FA (2015) J Am Chem Soc 137:8484-8489
28. Pavlov M, Siegbahn PEM, Blomberg MRA, Crabtree RH (1998) J Am Chem Soc 120:548-555
29. Lill SON, Siegbahn PEM (2009) Biochemistry 48:1056-1066
30. Volbeda A, Charon MH, Piras C, Hatchikian EC, Frey M, Fontecillacamps JC (1995) Nature 373:580-587
31. Matias PM, Soares CM, Saraiva LM, Coelho R, Morais J, Le Gall J, Carrondo MA (2001) J Biol Inorg Chem 6:63-81
32. Volbeda A, Fontecilla-Camps JC (2005) Coord Chem Rev 249:1609-1619
33. Fdez Galvan I, Volbeda A, Fontecilla-Camps JC, Field MJ (2008) Proteins 73:195-203
34. Ogata H, Kramer T, Wang H, Schilter D, Pelmenschikov V, van Gastel M, Neese F, Rauchfuss TB, Gee LB, Scott AD, Yoda Y, Tanaka Y, Lubitz W, Cramer SP (2015) Nat Commun 6:7890
35. Pardo A, De Lacey AL, Fernandez VM, Fan HJ, Fan YB, Hall MB (2006) J Biol Inorg Chem 11:286-306
36. Wu H, Hall MB (2008) CR Chim 11:790-804
37. Amara P, Volbeda A, Fontecilla-Camps JC, Field MJ (1999) J Am Chem Soc 121:4468-4477
38. Stein M, Lubitz W (2004) J Inorg Biochem 98:862-877

35. Pardo A, De Lacey AL, Fernandez VM, Fan HJ, Fan YB, Hall MB (2006) J Biol Inorg Chem 11:286-306
36. Wu H, Hall MB (2008) CR Chim 11:790-804
37. Amara P, Volbeda A, Fontecilla-Camps JC, Field MJ (1999) J Am Chem Soc 121:4468-4477
38. Stein M, Lubitz W (2004) J Inorg Biochem 98:862-877
39. Söderhjelm P, Ryde U (2006) J Mol Struc-Theochem 770:199-219
40. Ryde U, Nilsson K (2003) J Mol Struc-Theochem 632:259-275
41. Ryde U, Nilsson K (2003) J Am Chem Soc 125:14232-14233
42. Nilsson K, Ryde U (2004) J Inorg Biochem 98:1539-1546
43. Rod TH, Ryde U (2005) J Chem Theory Comput 1:1240-1251
44. Rod TH, Ryde U (2005) Phys Rev Lett 94:138302
45. Hu L, Eliasson J, Heimdal J, Ryde U (2009) J Phys Chem A 113:11793-11800
46. Hu L, Soederhjelm P, Ryde U (2011) J Chem Theory Comput 7:761-777
47. Hu L, Söderhjelm P, Ryde U (2013) J Chem Theory Comput 9:640-649
48. Sumner S, Söderhjelm P, Ryde U (2013) J Chem Theory Comput 9:4205-4214
49. Kaukonen M, Söderhjelm P, Heimdal J, Ryde U (2008) J Phys Chem B 112:12537-12548
50. Kaukonen M, Söderhjelm P, Heimdal J, Ryde U (2008) J Chem Theory Comput 4:985-1001
51. Delcey MG, Pierloot K, Phung QM, Vancoillie S, Lindh R, Ryde U (2014) Phys Chem Chem Phys 16:7927-7938
52. Ogata H, Nishikawa K, Lubitz W (2015) Nature 520:571-574
53. Olsson MHM, Søndergaard CR, Rostkowski M, Jensen JH (2011) J Chem Theory Comput 7:525-537
54. Gordon JC, Myers JB, Folta T, Shoja V, Heath LS, Onufriev A (2005) Nucleic Acids Res 33:W368-W371
55. Case DA, Berryman JT, Betz RM, Cerutti DS, Cheatham TE, III, Darden TA, Duke RE, Giese TJ, Gohlke H, Goetz AW, Homeyer N, Izadi S, Janowski P, Kaus J, Kovalenko A, Lee TS, LeGrand S, Li P, Luchko T, Luo R, Madej B, Merz KM, Monard G, Needham P, Nguyen H, Nguyen HT, Omelyan I, Onufriev A, Roe DR, Roitberg A, Salomon-Ferrer R, Simmerling CL, Smith W, Swails J, Walker RC, Wang J, Wolf RM, Wu X, York DM, Kollman PA, (2014), AMBER 14, University of California, San Francisco,
56. TURBOMOLE V65 2013, a development of University of Karlsruhe and Forschungszentrum Karlsruhe GmbH, 1989–2007, TURBOMOLE GmbH, since 2007; available from http://wwwturbomolecom,
57. Tao J, Perdew JP, Staroverov VN, Scuseria GE (2003) Phys Rev Lett 91:146401
58. Becke AD (1993) J Chem Phys 98:5648-5652
59. Becke AD (1988) Phys Rev A 38:3098-3100
60. Lee CT, Yang WT, Parr RG (1988) Phys Rev B 37:785-789
61. Schäfer A, Horn H, Ahlrichs R (1992) J Chem Phys 97:2571-2577
62. Weigend F, Ahlrichs R (2005) Phys Chem Chem Phys 7:3297-3305
63. Rappoport D, Furche F (2010) J Chem Phys 133:134105
64. Eichkorn K, Treutler O, Öhm H, Häser M, Ahlrichs R (1995) Chem Phys Lett 240:283-290
65. Eichkorn K, Weigend F, Treutler O, Ahlrichs R (1997) Theor Chem Acc 97:119-124
66. Ryde U (1996) Journal of Computer-Aided Molecular Design 10:153-164
67. Ryde U, Olsson MHM (2001) Int J Quantum Chem 81:335-347
68. Reuter N, Dejaegere A, Maigret B, Karplus M (2000) J Phys Chem A 104:1720-1735
69. Svensson M, Humbel S, Froese RDJ, Matsubara T, Sieber S, Morokuma K (1996) J Phys Chem 100:19357-19363
70. dftd3 software http://tocuni-muensterde/DFTD3/getd3html (accessed November 2012),
71. Maier JA, Martinez C, Kasavajhala K, Wickstrom L, Hauser KE, Simmerling C (2015) J Chem Theory Comput 11:3696-3713
72. Grimme S, Ehrlich S, Goerigk L (2011) J Comput Chem 32:1456-1465
73. Luzhkov V, Warshel A (1992) J Comput Chem 13:199-213
74. Heimdal J, Kaukonen M, Srnec M, Rulisek L, Ryde U (2011) Chemphyschem 12:3337-3347
75. Jorgensen WL, Chandrasekhar J, Madura JD, Impey RW, Klein ML (1983) J Chem Phys 79:926-935
76. Kampa M, Pandelia M-E, Lubitz W, van Gastel M, Neese F (2013) J Am Chem Soc 135:3915-3925
77. Jayapal P, Sundararajan M, Hillier IH, Burton NA (2008) Phys Chem Chem Phys 10:4249-4257